19th Brazilian Congress of Thermal Sciences and Engineering
November 6th–10th, 2022, Bento Gonçalves - RS - Brazil

ENC-2022-0250
NUMERICAL INVESTIGATION OF FE2O3-AL THERMITE REACTION USING ZERO AND FIRST-ORDER KINETIC MODELS

F. J. C. Pena
M. J. S. de Lemos
Departamento de Energia – IEME
Instituto Tecnológico de Aeronáutica - ITA
fabricio@ita.br; delemos@ita.br

Abstract. *The thermite reaction is a self-sustained exothermic reaction capable of producing high temperatures. Due to these features, this reaction has been employed in welding processes of railway tracks, material synthesis, pyrotechnics, ignition systems, etc. In this sense, this work proposes a numerical model to investigate the combustion behavior of a hematite/aluminum thermite reaction with zero and first-order kinetic models. As such, a constant kinetic rate is adopted for zero-order kinetics, whereas an Arrhenius equation based on the hematite consumption is considered for the first-order model. Also, the model considered the conjugate heat transfer and the species' melting during the reaction. The finite-volume method was employed to discretize and solve the governing equations. For that, a C++ algorithm was developed in the OpenFOAM software. It was found that a decrement in the pre-exponential factor and kinetic constant reduced temperatures and combustion front velocities. Experimental validation was performed by comparing numerical temperatures and combustion front velocities with data found in the literature. Results indicated a good agreement between numerical and experimental results for both models. Consequently, simulations indicated that employing either zero or first-order kinetics could produce similar results concerning temperatures and combustion velocities. However, the first-order model presented a difficult ignition and could not propagate the reaction with a low pre-exponential factor. Thus, the zero-order approach could be more feasible to investigate numerically thermite systems in which the primary focuses are the temperatures and combustion velocities.*

Keywords: *Combustion, Heat Transfer, Thermite, Kinetic Modeling, OpenFOAM*

1. INTRODUCTION

The hematite/aluminum thermite is a self-sustained exothermic reaction that generates high temperatures with reduced production of gases. Due to these features, this reaction has been employed in different industry sectors, where the most remarkable applications are found in railway tracks welding (Lonsdale and Engineer, 1999), self-propagating high-temperature synthesis of ceramic and composite materials (Wang *et al.*, 1993), pyrotechnics, and ignition systems (Kelly and Munger, 1991). Further, this reaction has been investigated in a new development to plug depleted oil wells (Pena and de Lemos, 2021; de Andrade *et al.*, 2021). This alternative method uses the energy produced by the chemical reaction to melt well components.

Due to the difficulty of experimentally measuring all factors that influence thermite combustion, simplified numerical models have been proposed to estimate peak temperatures, species concentrations, combustion front propagation, and some kinetic parameters. For instance, Brito *et al.* (2005) and Durães *et al.* (2006b) have simulated the experimental procedure performed by Durães *et al.* (2006a). In their numerical model, the authors assumed a one-dimensional domain and a zero-order kinetic to model the thermite reaction. Their simulations correctly estimated the combustion front velocities for a stoichiometric reaction, however, temperatures were extremely high and quite different from the experimental ones.

More recently, de Souza and de Lemos (2021) have expanded the above-mentioned model by using a first-order kinetic to simulate the thermite reaction. In this approach, the reaction was controlled by the hematite consumption, which was modelled by the Arrhenius equation. To evaluate their effects, kinetic parameters such as the activation energy and pre-exponential factor were varied. Based on these variations, the authors concluded that these kinetic parameters are extremely pivotal to correctly predict experiments. Most importantly, it was stated that these parameters are very singular to each thermite mixture, depending on the species involved and their equivalence ratio.

However, there is an absence of experimental studies that investigate the combustion behavior and also provide ex-

perimental kinetic parameters of a particular thermite reaction. The previous numerical models have been calibrating the kinetic parameters to match the experimental data. Assuming this calibration procedure and the absence of experimental kinetic parameters, it could be more feasible to use a zero-order kinetic model approach to estimate general parameters such as temperatures and combustion front velocities. Particularly, this approach could reduce computational time in simulations related to combustion applications where detailed kinetics is not the main focus.

In this sense, the present work investigates the experiment from Durães *et al.* (2006a) using zero and first-order kinetic models. Different from previous numerical works, this one assumes a two-dimensional axisymmetric domain with multiple layers, which accounts for the conjugate heat transfer between the thermite reaction and adjacent solid materials. In addition, this works models the phase change with a general enthalpy approach that accounts for the contribution of each species. We hope that the present investigation could collaborate to develop numerical models that simulate the thermite reaction in larger-scale combustion systems.

2. METHODOLOGY

2.1 Case description

This work investigates numerically the experimental procedure performed by Durães *et al.* (2006a). In this experiment, the authors prepared and characterized several mixtures to investigate the combustion behavior of different Fe_2O_3/Al thermite reactions. Assuming a stoichiometric composition, this thermite reaction can be described as

$$Fe_2O_3 + 2Al \longrightarrow 2Fe + Al_2O_3. \tag{1}$$

Also referring to the experiments from Durães *et al.* (2006a), reactants samples of 1-2 mm thickness were compressed between a stainless-steel disk and a PMMA (Polymethyl methacrylate) lid. According to Durães *et al.* (2006b), the mixture porosities varied from 0.3 to 0.5. The combustion was initiated through an ignition channel positioned at the disk center, and temperatures were measured by two thermocouples positioned at distinct radial positions. Based on these thermocouples responses, the combustion front velocity was measured. In addition, the radial flame propagation was evaluated by digital video-crono-photography.

Thermite combustion involves complex phenomena related to heat transfer, chemical kinetics, phase change and so on. Simulating all these phenomena is challenging and also demands a high computational demand. Thus, to simplify the experimental procedure from Durães *et al.* (2006a), the following assumptions are made: I) Azimuthal variations of scalars are neglected; II) Single-step and stoichiometric reaction; III) Zero and first-order kinetics; IV) Porosity is considered constant during the whole reaction and is only used to calculate the thermal properties of the mixture; V) Radiative heat transfer inside the thermite region is not considered; VI) The phase change is only considered inside the thermite region; VII) Phase changes are exclusively related to the melting and solidification phenomena; VIII) The movements related to the liquid phase are not considered.

Under such circumstances, the present model assumes a two-dimensional axisymmetric domain with multiple layers, as illustrated in Figure 1.

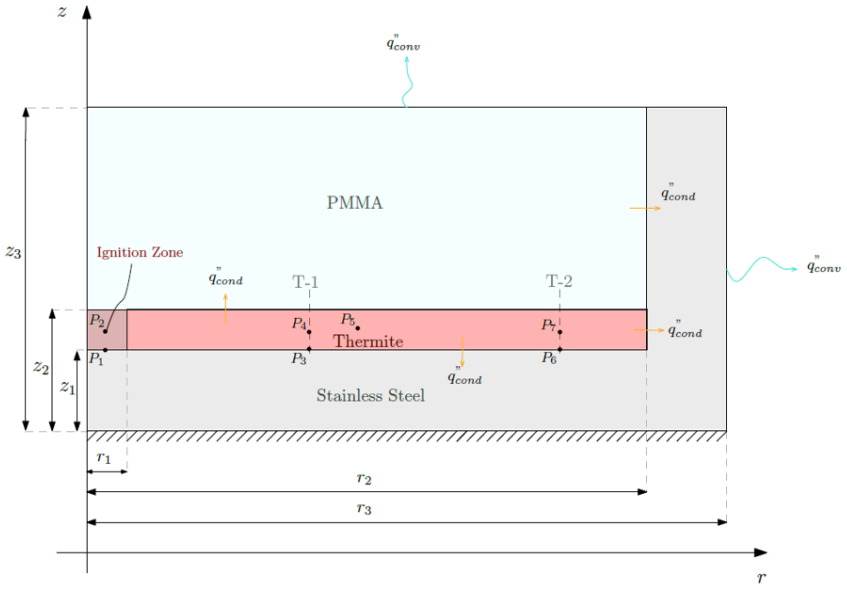

Radius	Dimension [m]
r_1	0.0015
r_2	0.025
r_3	0.03
Length	**Dimension [m]**
z_1	0.005
z_2	0.0065
z_3	0.015

Point	Position (r,z) in [m]
P_1	$(0.00075, 0.005)$
P_2	$(0.00075, 0.00575)$
P_3	$(0.01, 0.005)$
P_4	$(0.01, 0.0062)$
P_5	$(0.0125, 0.00575)$
P_6	$(0.02, 0.005)$
P_7	$(0.02, 0.0062)$

Figure 1. Computational domain.

2.2 Species Equations

Similarly to the previous numerical works that simulated the same problem presented here, this work assumes the species conservation without diffusion and advection, which results in

$$\frac{\partial(\rho_m Y_i)}{\partial t} = R_i \tag{2}$$

where ρ_m is the mixture density, Y_i is the mass fraction and R_i is the net rate of production of species i. For the sake of simplicity, the species Fe_2O_3, Al, Fe and Al_2O_3 will be further identified, respectively, by subscripts A, B, C and D. Next, Eq.(2) can be represented in the following form

$$\frac{dW_i}{dt} = \alpha_i \dot{r}. \tag{3}$$

In Eq.(3), W_i represents the concentration and α_i stands for the stoichiometric coefficient of species i. Also, $\dot{r}$ represents the chemical kinetic rate, which will be discussed later. Applying a explicit discretization to Eq.(17) yields

$$W_i^t = W_i^{t-1} + \alpha_i \dot{r} \tag{4}$$

where t denotes a certain time. It is also important to mention that the stochiometric coefficient of reactants is negative, indicating that they are being consumed.

2.2.1 Zero-order kinetic

The reaction rate,$\dot{r}$, usually has individual value for each chemical species. In order to simplify the chemical model, zero and first-order kinetic models are assumed here. As such, a zero-order kinetic assumes a constant value for the kinetic rate, which is does not depend on the concentration of any chemical species. For this model, the reaction rate can be described by

$$\dot{r} = K_c \tag{5}$$

where K_c is a constant value in kg/(m³s).

2.2.2 First-order kinetic

In a kinetic first-order model, the reaction rate depends on the concentration of only one species. Here, the model depends on the consumption. Based on the formulation presented by de Souza and de Lemos (2021), the first-order kinetic rate reads as

$$\dot{r} = W_A^t A_F e^{\frac{-E_A}{RT}} \tag{6}$$

where A_F is the pre-exponential factor in s^{-1} and E_A is the activation energy in kJ/mol. Finally, R is the ideal gas constant.

2.3 Energy Equations

As displayed back in Fig. 1, the present model accounts for different regions. For the solid regions representing the PMMA and stainless steel, only heat diffusion is assumed. Thus, the energy equation in these two regions reads as

$$\rho_s c_{p,s} \frac{\partial T}{\partial t} = \nabla \cdot (k_s \nabla T) \tag{7}$$

where ρ_s is the density, $c_{p,s}$ is the specific heat and k_s is the thermal conductivity for the solid regions. These properties are considered constants for both materials and were obtained in the literature (Kim, 1975; L.Shi *et al.*, 2015). For the thermite reaction, the species phase change and heat generated by the reaction are included and, therefore, the energy equation reads as

$$\rho_m c_{p,m} \frac{\partial T}{\partial t} = \nabla \cdot (k_m \nabla T) + S_g + S_h \tag{8}$$

where $c_{p,m}$ and k_m are the specific heat and thermal conductivity of the mixture, respectively. S_g is the source term representing the heat generated by the reaction, whereas S_h represents the species phase change. The procedure to calculate these source terms will be discussed next.

2.3.1 Phase change model

The phase change model employed here assumes a static melting and solidification of the chemical species, without including the convective effects. Also, the model does not include the species evaporation due to the high temperatures produced by the thermite combustion. Having said that, this work uses the enthalpy method (Voller and Prakash, 1987) and expands it to multi-species approach that considers the phase change of each species. The only exception was the hematite (Fe_2O_3), which decomposes to other iron oxides (Durães *et al.*, 2007).

As described in Eq.(5), the general source term method (Voller and Swaminathan, 1991) is applied to incorporate the phase change into the energy equation. Hence, this source term S_h can be defined as

$$S_h = -\frac{\partial(\rho_m \Delta h_{L,m})}{\partial t} \tag{9}$$

where $\Delta h_{L,m}$ is the latent heat of the mixture and is calculated through the mixture's rule as follows

$$\Delta h_{L,m} = \sum_i Y_i \Delta h_{L,i} \tag{10}$$

in which $\Delta h_{L,i}$ is the latent heat of an individual species i. Considering the same species i, it is possible to associate the latent heat $\Delta h_{L,i}$ and the latent heat of fusion L_i, resulting in

$$\gamma_i = \frac{\Delta h_{L,i}}{L_i} \tag{11}$$

where γ_i stands for the liquid fraction the species i.

The thermite species are pure substances and, therefore, their melting is occurs at an exact temperature. However, this isothermal phase change is commonly modeled with a small temperature range, which creates a small mushy zone that is composed of both liquid and solid phases. In this work, the mushy zone is delimited by a temperature interval of 2 K. Thus, the relation between the temperature and the liquid fraction(γ_i) can be defined as

$$\gamma_i = \begin{cases} \dfrac{\Delta h_{L,i}}{L_i} = 0, & \text{if } T < T_{S,i} \\ \dfrac{\Delta h_{L,i}}{L_i} = 1, & \text{if } T > T_{L,i} \\ \dfrac{\Delta h_{L,i}}{L_i} = \dfrac{T - T_{S,i}}{T_{L,i} - T_{S,i}}, & \text{if } T_{S,i} < T < T_{L,i} \end{cases} \tag{12}$$

where $T_{S,i}$ and $T_{L,i}$ are the solidus and liquidus temperatures of a certain species i, respectively. It is also important to mention that the first two lines are known, respectively, as undershoot and overshoot corrections. These corrections facilitate the convergence by updating the liquid fraction, avoiding values below 0 and above 1. The last line represents the linear relation between the temperature and the liquid fraction inside the mushy zone.

2.3.2 Heat generation

In this work, the heat generated by the reaction is incorporated to the energy equation through the source term S_g. This source term is directly related to the reaction enthalpy, Q, and to the reaction kinetic rate,$\dot{r}$, as follows

$$S_g = -Q\dot{r} \tag{13}$$

where the terms Q and are given in J/kg and kg/m³.s, respectively. The multiplication of these terms yields a source term with units in W/m³, as is commonly implemented in the energy equation. The literature states that the reaction enthalpy is calculated considering the enthalpy variation of products and reactants. Hence, the reaction enthalpy is equal to

$$Q = \sum_i (h^0_{f,i} + h_{s,i} + \Delta h_{L,i}) \tag{14}$$

where $h_{s,i}$ is the sensible enthalpy and $h^0_{f,i}$ is the enthalpy of combustion of a species i. It is important to remind that Q is negative in a exothermic reaction.

2.4 Thermal properties

The thermal properties used in this work are presented in Table 1. From this table, one can observe that constant properties were primarily applied for the solid regions. On the other hand, some thermite thermal properties were temperature-dependent. Regarding that, it is important to mention that porosity affect the mixture thermal properties and, therefore,

the thermal properties of the air must be considered. Thus, Fig.2 shows the temperature dependent thermal properties used in this work. The analysis was restricted to 3500 K and these properties were extracted from the data found in the literature (Brito *et al.*, 2005; Chase, 1998; Molgaard and Smeltzer, 1971).

Table 1. Thermal properties used in simulations.

Material	Thermite					PMMA	Stainless Steel AISI 304
	Fe2O3	Al	Fe	Al2O3	Air		
Specific Heat [J/kg.K]	Fig. 2a	Fig. 2a	Fig. 2a	Fig. 2a	Fig. 2a	1500	510
Thermal Cond. [W/m.K]	5.9	Fig. 2b	Fig. 2b	Fig. 2b	Fig. 2b	0.16	13
Density [kg/m³]	5062.3	Fig. 2c	Fig. 2c	3975	Fig. 2c	1202.9	7894
Solidus Temperature [K]	-	932	1809	2344	-	-	-
Liquidus Temperature [K]	-	934	1811	2346	-	-	-
Latent heat of fusion [J/kg]	-	387672	271956	1161296	-	-	-

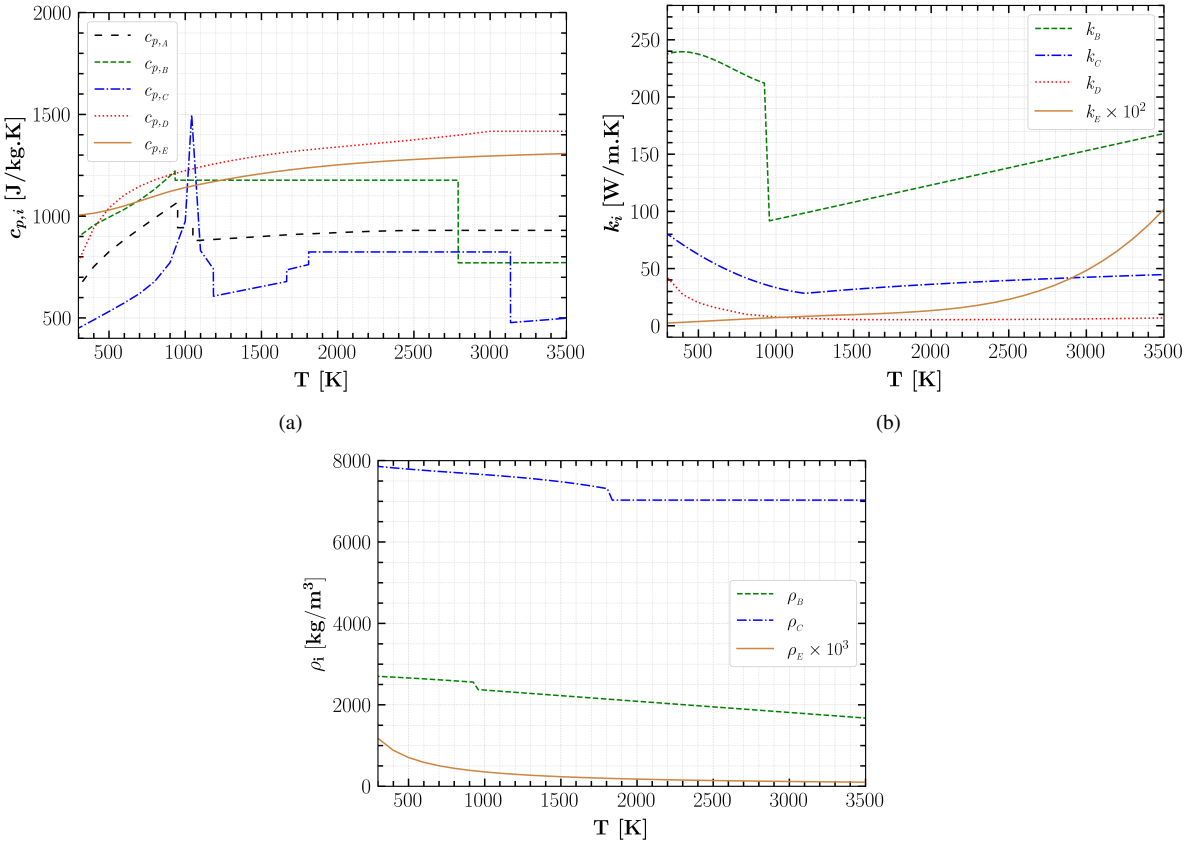

Figure 2. Thermal properties varying with temperature: (a) specific heat, (b) thermal conductivity and (c) density.

The above-mentioned properties can be estimated through the mixture rule. Based on the equations proposed by , the specific heat and density can be calculated by

$$c_{p,m} = \sum_i Y_i c_{p,i} \qquad \text{for } i = A, B, C, D, E; \tag{15}$$

$$\rho_m = \sum_i \upsilon_i \rho_i \qquad \text{for } i = A, B, C, D, E; \tag{16}$$

where υ_i is the volume fraction for a certain species i and E represents the air. Next, the thermal conductivity is estimated by using an average between the serial and parallel arrangement of components (Brito *et al.*, 2005). Thus, the thermal

conductivity of the mixture reads as

$$k_m = \frac{\dfrac{1}{\sum_i \dfrac{\upsilon_i}{k_i}} + \sum_i \upsilon_i k_i}{2} \qquad \text{for } i = A, B, C, D, E. \tag{17}$$

2.5 Numerical Schemes

The solver developed in this work is based on the *chtMultiRegionFoam*, which calculates the conjugate heat transfer through solid and fluid regions. This solver uses a segregated solution as general equations are solved sequentially and an iterative scheme is applied to simulate the thermal coupling between regions. Here, the fluid regions is replaced by a thermite region. Therefore, equations are initially solved in this region and then the energy equation is solved in the solid regions.

The numerical scheme employed to discretize the governing equations is the control volume approach. Concerning spatial discretization, scalars are computed through a second-order central difference scheme, and the least square method is used to calculate the gradients. The temporal term of the energy equation is discretized by a second-order accurate backward Euler scheme. On the other hand, an explicit discretization was employed to compute the species' concentrations W_i.

3. RESULTS

3.1 Grid and Time-step analyses

Figure 3 shows the grid structure for the model depicted in Fig.1. The computational domain was divided in 6 blocks to guarantee a refined grid in certain regions. Blocks I and II represent, respectively, the grid of the PMMA and the thermite regions, whereas the remaining blocks are related to grid of the stainless-steel layer. It can also be observed that a greater refinement is employed in the interfaces of the thermite region (Block II), since this area presents a greater thermal gradient due to the high temperatures generated by the reaction and the contact with other materials. Next, the solution independency related the grid size was investigated. Grid sizes with 125 x 80, 240 x 140, 440 x 150, 640 x 160, 840 x 160 and 1540 x 200 nodes were assessed. Using both zero-order and first-order kinetic models, results have not changed from 640 x 160 nodes on and, therefore, this grid configuration was employed in further simulations.

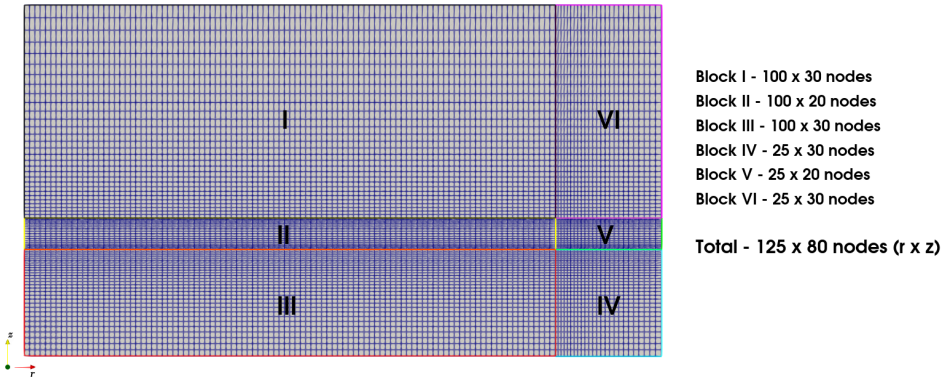

Figure 3. Grid structure.

Similarly, an independency study related to the time-step size was employed. Figure 4 shows temperature profiles calculated with different time-steps sizes and kinect orders at position P_5 (see Fig.1). In Fig.4a, a zero-order kinetic model with $K_c = 95000$ kg/(m³s) was used to compare temperature with time-steps ranging from 10^{-3} to 10^{-6} s. One can observe that simulations produced similar result with $dt = 10^{-5}$ s and $dt = 10^{-6}$ s. Still, results with $dt = 10^{-4}$ s only shows a small difference in the combustion front velocity, indicating that might be feasible to use this higher time-step with this kinetic model. On the other hand, Fig.4b displays temperature profiles for simulation that used a first-kinect order with $A_F = 9.4E + 05\ s^{-1}$. It can be observed that the solution presented a slightly greater dependency on the the time-step size for this kinetic model. For instance, results for $dt = 10^{-3}$ s are not displayed because the reaction has not propagated with this time-step size. In addition, the difference between temperature profiles with $dt = 10^{-4}$ s is remarkable when compared with lower time-steps results. For the present case, which simulates only 1 second, the computational costs arising from a lower time-step might not be significant. In this sense, simulations will use $dt = 10^{-5}$ s for both kinetic models.

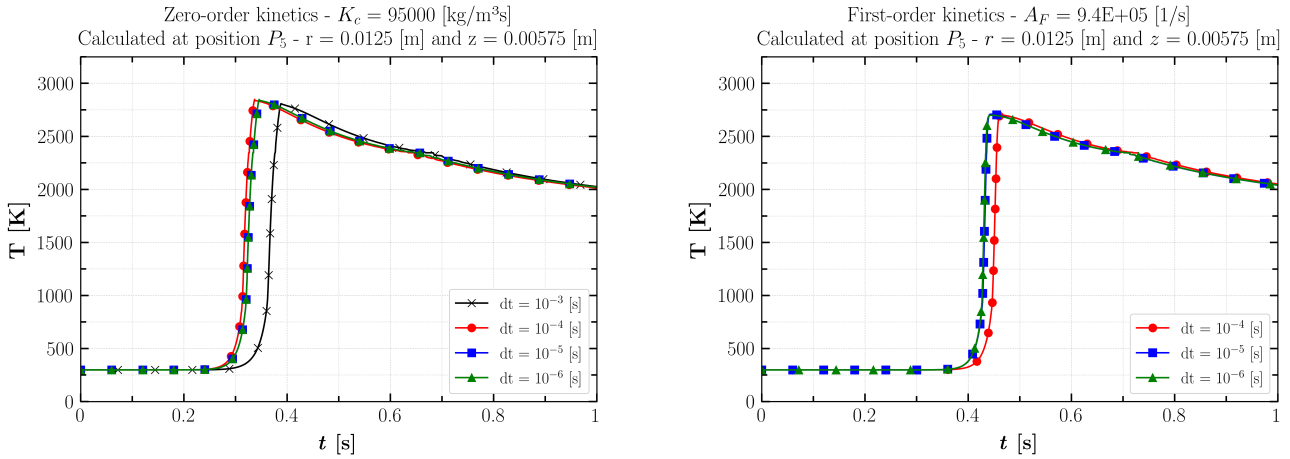

(a) (b)

Figure 4. Calculated temperature profiles with different time-step sizes at position P_5. Results with (a) zero-order and (b) first-order kinetic models.

3.2 Velocity calibration

In order to compare both kinetic models, the combustion front velocities (v) are calibrated until they were close to the experimental ones measured by Durães *et al.* (2006a). In their work, the authors measured the combustion velocities with different methodologies, including one that was based on difference between the thermocouples responses. These thermocouples were positioned at $r = 0.01$ and 0.02 m. In the present numerical work, the velocities are measured by the difference between the maximum peak temperatures at the last-mentioned radial positions. As these maximum peaks are observed at $z = 0.0062$ m, velocities are estimated between positions P_4 and P_7 (see Fig.1). Further, the kinetic parameters are varied to calibrate the combustion front velocities. For the zero-order kinetic model, K_c varied from 60000 to 100000 kg/(m³s). Regarding the first-order kinetic model, Eq.(6) describes that the reaction rate depends on both E_A and A_f. An experimental E_A of 158 kJ/mol was obtained by Sahoo *et al.* (2017) and, therefore, this constant value was applied. On the other hand, experimental pre-exponential factors for the thermite reaction are scarce on the literature. Based on the calibration performed by de Souza and de Lemos (2021), this work varied A_F from $2.2E+06$ to $9.4E+05\ s^{-1}$.

Figures 5a and b show the combustion front velocities varying with K_c and A_F, respectively. It is observed in Fig.5a that the velocity increases as K_c is incremented. Most importantly, the zero-order model presents a close combustion front velocity to the experimental one when $K_c = 85000$ kg/(m³s). Next, Fig.5b shows velocities increasing by enhancing the values of A_F for simulations with a first-order kinetic model. However, this trend is way more remarkable when compared to the results with a zero-order model. Also, combustion velocities were close to the experimental data with $A_F = 9.4E+05\ s^{-1}$. Below this pre-exponential factor, the reaction has not propagated for this numerical model, indicating that the zero-order model present less limitations when varying kinetic parameters.

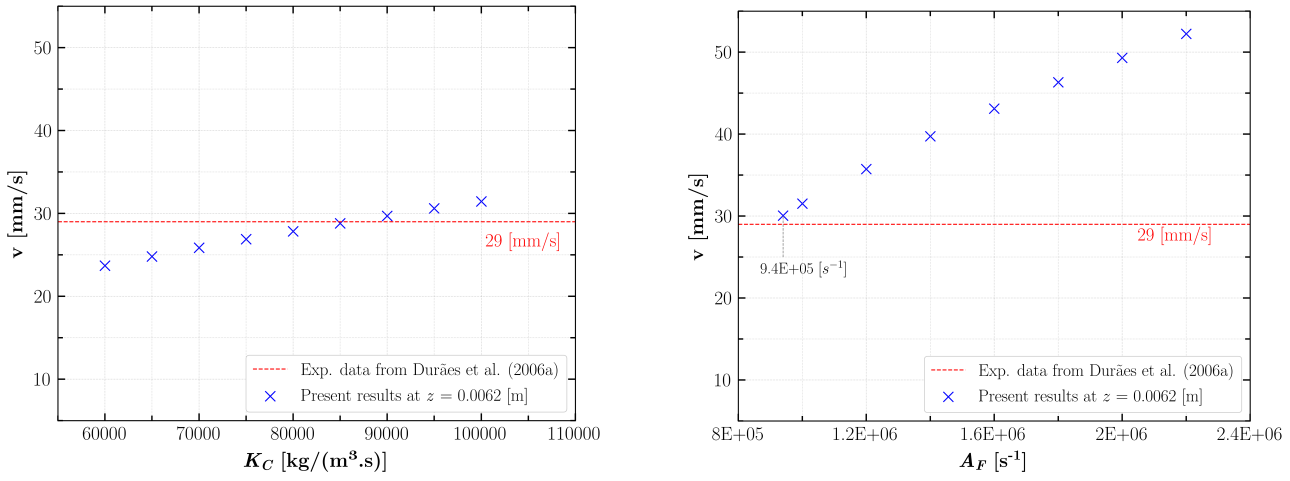

(a) (b)

Figure 5. Combustion front velocities varying with (a) K_c and (b) A_F.

3.3 Maximum peak temperatures

Figure 6 shows maximum peak temperatures varying with K_c and A_F at different radial positions. For both models, maximum temperatures increased as the kinetic parameter were enhanced. Specifically, Fig. 6a displays that the numerical model with zero-order kinetics presented peak temperatures closer to the experimental data measured at $r = 0.01$ m. Also, the peak temperatures at the two distinct positions were pratically the same. For a calibrated combustion velocity with $K_C = 85000$ kg/(m³s), numerical temperatures were 7.66 K higher at $r = 0.01$, while they were 89.14 K lower at $r = 0.02$ m when compared to the experimental data. On the other hand, Fig. 6b demonstrates that the numerical peak temperatures with a first-kinetic model were slightly higher than the ones obtained with the other kinetic model. The peak temperatures at the two positions presented a more notable difference, which differs from the trend presented in Fig. 6a. Comparing the simulation that used $A_F = 9.4E + 05\ s^{-1}$ with the experimental data, numerical peak temperatures were 6.87 K higher and 82.33 K lower at $r = 0.01$ and 0.02 m, respectively.

In order to compare the kinetic models that had similar combustion velocities, simulations with $K_C = 90000$ kg/(m³s) and $A_F = 9.4E + 05\ s^{-1}$ are taken into account. At position P_4, peak temperatures were 2749.93 and 2739.02 K for the zero and first-order kinetic models, respectively. Similarly, these temperatures were 2762.67 and 2756.89 K at position P_7. Hence, even for a similar combustion front velocity, the first-order kinetic model produces higher temperatures. In addition this model presented a higher temperature increment between radial positions, which is a behavior observed in the experiments from Durães *et al.* (2006a).

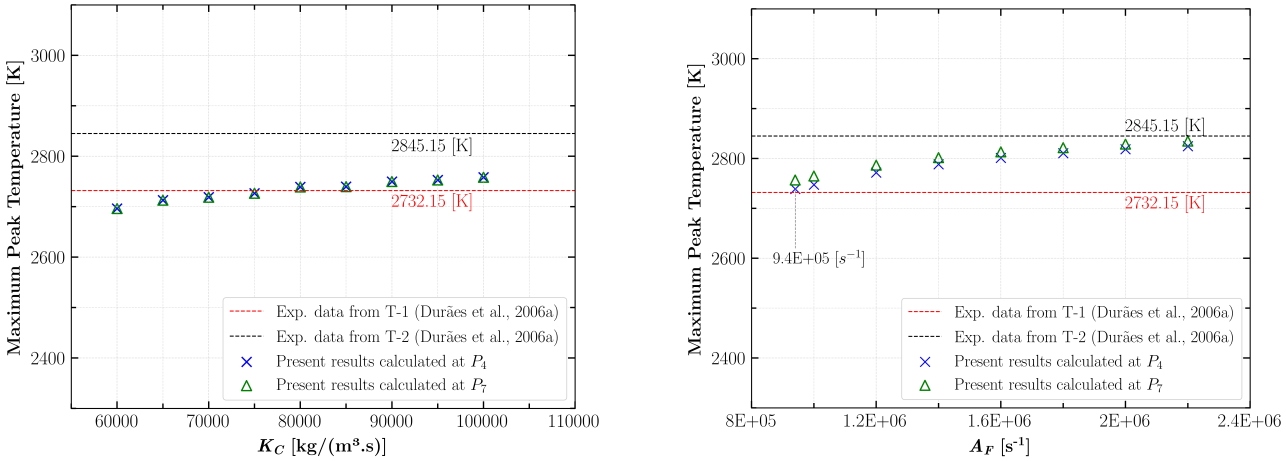

Figure 6. Maximum peak temperatures varying with (a) K_c and (b) A_F.

Overall, both models presented temperatures close to the experimental ones when the combustion front velocities were calibrated. However, the zero-order model could produce closer values due to its feasibility to simulate reactions with lower combustion front velocities. This feasibility is possibly related to the ignition procedure, which will be discussed next.

3.4 Ignition behavior

Figure 7 shows the hematite mass fraction, Y_A, varying with time at positions P_1 and P_2. These points are located at the same radial position inside the ignition zone and only differs longitudinally. Having said that, Fig. 7a shows over time for a zero-order kinetic model with $K_C = 95000$ kg/(m³s). As expected, the hematite consumption presented a linear behavior due to the zero-order approach. In addition, the consumption was similar at both positions, indicating a uniform ignition. On the other hand, Fig. 7a shows different results for the first-order model with $A_F = 9.4E + 05\ s^{-1}$. It can be observed a curved behavior during the hematite consumption, which was also expected. Further, the ignition was non-uniform as a delay observed at position P_1. This trend is related to the temperature dependence described in Eq.(6) and to higher heat losses observed around next to the thermite-steel interface. It can be noted in Tab.1 that the stainless-steel disk has a higher thermal conductivity when compared to the PMMA lid, which mostly works as a insulating material. Thus, lower temperatures are expected at position P_1 and, consequently, lower reaction rate and heat generation. Ultimately, these lower values complicate the combustion ignition around this area and the reaction propagation with lower pre-exponential factors.

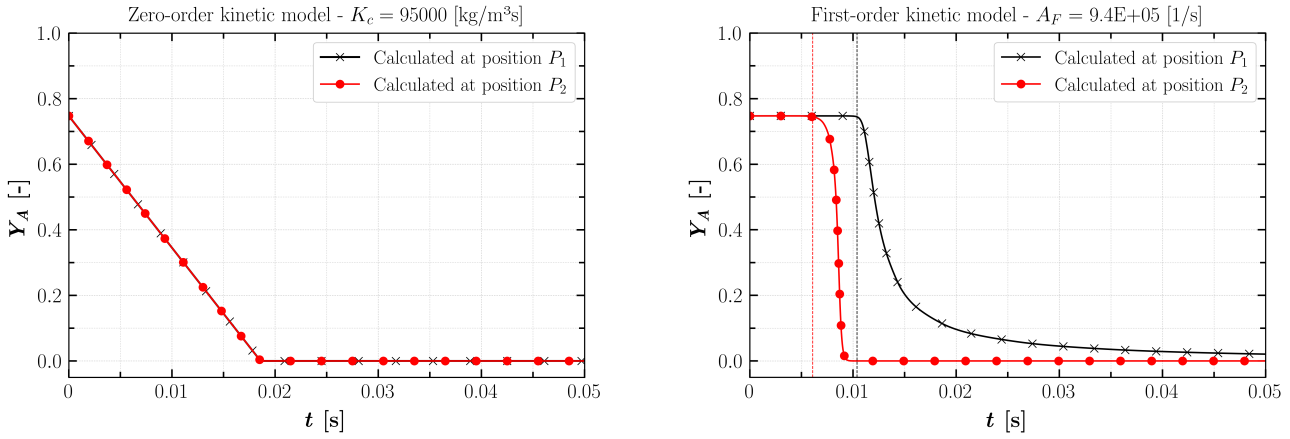

(a) (b)

Figure 7. Y_A consumption over time at positions P_1 and P_2. Results concerning simulations with (a) zero and (b) first-order kinetic models.

4. CONCLUSIONS

This work has investigated a Fe2O3/Al thermite reaction propagation in a disk-shaped geometry, which was approached as a two-dimensional domain with multiple layers, including the thermite mixture and adjacent solid materials. A finite volume solver was developed inside *OpenFOAM*® to simulate the chemical reaction, conjugate heat transfer and species' phase change.

Regarding the chemical modeling, zero and first-order kinetic models were employed. These models were calibrated with experimental data and results were compared. Based on these results, the following conclusions are made:

- The grid size dependence for both models was similar. On the other hand, the first-order kinetic model presented a slightly greater dependence related to the time-step size when compared to the zero-order model;
- Numerical maximum peak temperatures presented a good agreement with experimental data. Particularly, results with the zero-order model were slightly close to experimental peak temperatures. In addition, this model comfortably varied the combustion velocities, while the first-order model displayed difficulties to produce lower velocities;
- The hematite consumption is better represented with a first-order approach, as the zero-order kinetics shows a simple linear consumption;
- Different ignition behaviours were observed for each kinetic model. The zero-order model presented a uniform ignition, whereas a non-uniform trend was noticed with first-order kinetics. Regarding the latter, the non-uniform ignition produces a delay next to the thermite-steel interface and imposes an hindrance to the reaction propagation;
- The zero-order model can reproduce experimental combustion velocities and peak temperatures with less computational costs. Further, the variation of parameters presented less limitations when compared with the first-order model. Therefore, assuming a large-scale combustion application that only demands the heat generated by a thermite reaction, the zero-order model could be a more feasible approach.

5. ACKNOWLEDGEMENTS

The authors are thankful to PETROBRÁS, for their invaluable support during the preparation of this work.

6. REFERENCES

Brito, P., L.Durães, J.Campos and A.Portugal, 2005. "Modelling and simulation of fe2o3/aluminum thermite combustion". In *Proceedings of the 9th International Chemical Engineering Conference*. Coimbra, Portugal.

Chase, M.W., 1998. *NIST-JANAF thermochemical tables*, Vol. 9. American Chemical Society Washington, DC.

de Andrade, G.S., de Lemos, M.J. and Colombo, D., 2021. "A new hybrid analytical/numerical method for transient heat conduction in composite hollow cylinders applied to plug and abandonment of oil wells". *International Journal of Thermal Sciences*, Vol. 168, p. 106981.

de Souza, K.M. and de Lemos, M.J., 2021. "Detailed numerical modeling and simulation of fe2o3- al thermite reaction". *Propellants, Explosives, Pyrotechnics*, Vol. 46, No. 5, pp. 806–824.

Durães, L., Brito, P., Campos, J. and Portugal, A., 2006b. "Modelling and simulation of fe2o3/aluminum thermite combustion: experimental validation". In *Computer Aided Chemical Engineering*, Elsevier, Vol. 21, pp. 365–370.

Durães, L., Costa, B.F., Santos, R., Correia, A., Campos, J. and Portugal, A., 2007. "Fe2o3/aluminum thermite reaction intermediate and final products characterization". *Materials Science and Engineering: A*, Vol. 465, No. 1-2, pp. 199–210.

Durães, L., J.Campos and A.Portugal, 2006a. "Radial combustion propagation in iron(iii) oxide/aluminum thermite mixtures". *Propellants, Explosives, Pyrotechnics*, Vol. 31, No. 1, pp. 42–49.

Kelly, M.D. and Munger, A.C., 1991. "Ignitor with stable low-energy thermite igniting system". US Patent 4,989,515.

Kim, C.S., 1975. "Thermophysical properties of stainless steels". Technical report, Argonne National Lab., Ill.(USA).

Lonsdale, C. and Engineer, M., 1999. "Thermite rail welding: history, process developments, current practices and outlook for the 21st century". In *Proc. AREMA 1999 Annu. Conf.* Citeseer, Vol. 1895, p. 18.

L.Shi, M.Chew, V.Novozhilov and P.Joseph, 2015. "Modeling the pyrolysis and combustion behaviors of non-charring and intumescent-protected polymers using "firescone"". *Polymers*, Vol. 7, No. 10, pp. 1979–1997.

Molgaard, J. and Smeltzer, W., 1971. "Thermal conductivity of magnetite and hematite". *Journal of applied physics*, Vol. 42, No. 9, pp. 3644–3647.

Pena, F.J. and de Lemos, M.J., 2021. "Unsteady heat conduction with phase change applied to a novel thermal plug and abandonment process". *International Journal of Thermal Sciences*, Vol. 170, p. 107155.

Sahoo, S., Danali, S. and Arya, P., 2017. "Ignition behavior of al/fe2o3 metastable intermolecular composites". *Int. J. Eng. Res. Sci*, Vol. 3, No. 11, pp. 61–71.

Voller, V.R. and Prakash, C., 1987. "A fixed grid numerical modelling methodology for convection-diffusion mushy region phase-change problems". *International journal of heat and mass transfer*, Vol. 30, No. 8, pp. 1709–1719.

Voller, V.R. and Swaminathan, C., 1991. "Eral source-based method for solidification phase change". *Numerical Heat Transfer, Part B Fundamentals*, Vol. 19, No. 2, pp. 175–189.

Wang, L., Munir, Z. and Maximov, Y.M., 1993. "Thermite reactions: their utilization in the synthesis and processing of materials". *Journal of Materials Science*, Vol. 28, No. 14, pp. 3693–3708.

7. RESPONSIBILITY NOTICE

The authors are solely responsible for the printed material included in this paper.